Hindawi
Journal of Chemistry
Volume 2022, Article ID 6505556, 15 pages
https://doi.org/10.1155/2022/6505556

Research Article

Kinetics and Thermodynamics of β-Carotene Adsorption onto Acid-Activated Clays Modified by Zero Valent Iron

J. Nga,[1] J. Avom,[1] J. Tonga Limbe,[1] D. Ndinteh,[1] H. L. Assonfack,[1] and C. M. Kede [2,3]

[1]*Department of Chemistry, Faculty of Science, University of Yaounde I, P.O. Box 812, Yaounde, Cameroon*
[2]*Department of Process Engineering, National Higher Polytechnic School of Douala, University of Douala, P.O. Box 2701, Douala, Cameroon*
[3]*Department of Chemistry, Faculty of Science, University of Douala, P.O. Box 24175, Douala, Cameroon*

Correspondence should be addressed to C. M. Kede; meleack@yahoo.fr

Received 27 February 2022; Accepted 8 August 2022; Published 10 October 2022

Academic Editor: Rabia Rehman

Copyright © 2022 J. Nga et al. This is an open access article distributed under the Creative Commons Attribution License, which permits unrestricted use, distribution, and reproduction in any medium, provided the original work is properly cited.

The adsorption of β-carotene from crude palm oil onto acid-activated clay and clay modified by zero valent iron (ZVI) was investigated in this work. Spectroscopic studies including FTIR, XRD, and SEM were used for its characterization. The adsorption characteristics such as kinetics, mechanism, isotherms, and thermodynamics of β-carotene were studied. The kinetic data were analyzed using the pseudo-first-order kinetic equation, pseudo-second-order kinetic equation, and intraparticle diffusion model. The pseudo-second-order kinetic model is the only one that describes the experimental data well ($R^2 \geq 0.969$). The chemical analysis of bulk clay showed that the predominant oxides are Al_2O_3 (57.91 wt%), Fe_2O_3 (32.54 wt%), SiO_2 (3.09 wt%), K_2O (2.37 wt%), and CaO_2 (1.73 wt%). The adsorption capacity increases with an increase in temperature. The equilibrium data were described better by the Freundlich model for all clays. To determine the best fit kinetic model for each system, three error analysis methods, namely, chi-square (χ^2), residual mean squared error (RMSE), and mean percent error (%APE) were used to evaluate the data. A thermodynamic study demonstrated that β-carotene adsorption is spontaneous, endothermic, and an entropy driven process for both forms of clay.

1. Introduction

Palm oil is mainly composed of fatty acids called triglycerides and minor constituents such as carotenoids (β-carotene), vitamin E (tocopherols and tocotrienols), phytosterols, phospholipids, glycolipids, and squalene [1]. Its orange-yellow color is due to its high content of carotenoids [2]. The other minor constituents are in low concentration [3]. Each constituent has a specific role in palm oil-based food [4]. β-Carotene is known as provitamin A and has a useful interest as a vitamin A source in human nutrition [5–7]. However, during long-term storage and conservation, this constituent (like others) may undergo chemical transformations under the actions of light, oxygen, and high temperatures [8]. These reactions cause the oils to become acidic and give them an undesirable taste and flavor [9]. Refining is one of the most widely used techniques for improving the quality of domestic oils [10]. It is done in four steps: degumming, neutralization, bleaching, and deodorization [11]. Degumming eliminates phospholipids, gums, and mucilages [12]. Neutralization removes free fatty acids [13]. Deodorization removes volatile compounds such as aldehydes, ketones, and alcohols [14]. Bleaching, the most important step, removes pigments, oxidation products, and trace of metals [11]. It improves the appearance, taste, and flavor of oil [15, 16]. In this step, the use of bleaching earth is usual. The bleaching earths are usually clay materials with improved adsorption properties. The improvement of the adsorption capacity is usually achieved through acidic activation of clay materials [9, 17–19]. In the case of kaolinite, activation is mandatory, given that this type of clay usually exhibits small specific area. Acid treatment of kaolinite leads to the leaching of Al^{3+} from the structure which results in improved porosity of the clay. Also, upon severe acid

treatment (high concentration as from 5 N), the formation of an amorphous silica gel is observed. These changes lead to changes in the specific surface area and porosity [20]. Acid treatment also increases the proportion of mesopores in the range of 3–4.5 nm, which has been proposed to be suitable for the adsorption of pigments on the clay [19–21].

Also, the improvement of kaolinite adsorption capacity is possible through composite material elaboration. To this end, the use of nanoparticles is of particular interest given that such particle exhibits high specific areas in comparison to micrometric particles [22, 23].

The objective of the present study is to improve the adsorption capacity of a clay for the removal of beta-carotene from palm oil. To this end, a clay was activated by moderate acid treatments and the acid-activated sample was also doped by zero valent iron (ZVI) nanoparticles. Both the acid-activated and ZVI-doped acid-activated clay were used in batch tests for the removal of β-carotene from palm oil. The raw clay sample and its derivatives were characterized using X-ray diffraction (XRD), Fourier transformed infrared (FTIR), and scanning electron microscopy (SEM). The adsorption test on the raw clay was done in comparison to the acid-activated and acid-activated doped with ZVI. The adsorption results were analyzed using adsorption models including Langmuir, Freundlich, and Temkin isotherms. In order to get an insight on the adsorption mechanism, some kinetics models were also evaluated.

2. Materials and Methods

2.1. Clay Sample Location and Conditioning. The clay used in this study was collected in Mbembe, a locality of the Bot-Makak subdivision (center region of Cameroon). The GPS coordinates of the sampling location are 4°10′77″N and 11°00′.44″E. The sample was grounded in a mortar and sieved over 125 μm mesh. The sieve sample is stored in a polyethylene bag before its use.

2.2. Acid Treatment of the Clay. Analytical grade sulfuric acid has been used for the preparation of acidic solutions in distilled water. The acid-treated samples were obtained as follows: 25 g of clay is mixed with 100 ml of 4 N sulfuric acid solution for 30 min and at a temperature of 90°C. The mixture obtained was cooled to room temperature before being filtered to collect the clay cake (ACMB493). This cake was repeatedly washed with hot distilled water until the filtrate is tested free of sulfate ions and then dried in an oven at 105°C.

2.3. Preparation of the Zero Valent Iron-Doped Clay Samples. In this preparation (Figure 1), zero valent iron were obtained through a reduction of a solution iron (II) using a polyphenol extract from green tea.

To obtain ZVI MB 493, 4 g of ACM B493 was added to a solution of ZVI and then stirred for 1 h. The ZVI MB 493 were separated and washed many times with water and dried. The confirmation of a composite formation made of clay and zero valent iron is done using XRD.

2.4. Characterization of Clays and ZVI/Clays. The mineralogy of clays was determined using a Philips diffractometer with PW1710 control unit operating at 40 kV and 30 mA using the Ni-filtered Cu-Kα radiation. The diffractograms were automatically matched with JCPDS cards in the computerized XRD CD-ROM. Bulk mineralogy was studied with randomly oriented air-dried samples. XRD hot stage analysis was reported to have identified thermally stable polymorph of the clays and nZVI/clays. For the determination of the qualitative and quantitative powder macrocomposition by XRF analysis, an energy-dispersive XRF spectrometer model ElvaX Light SDD was used. The XRF spectrometer was equipped with an X-ray tube with a Rh anode operating at a voltage of 50 kV and a fast SSD detector, which provides a resolution of <140 eV for the Mn Kα-line.

Samples were prepared by homogeneously mixing 1 mg of sample with 100 mg of KBr and then pressing into pellets for study by diffuse reflective infrared Fourier transform (DRIFT) spectroscopy. Diffuse reflectance infrared Fourier transform spectra were measured with a Perkin Elmer Fourier transform infrared spectrometer (Spectrum One) operating in the mid-IR spectrum range (4000–450 cm^{-1}), for a resolution of 4 cm^{-1}. Morphological analysis of the samples was performed by field emission scanning electron microscopy (FE-SEM) using a JEOL JSM-7600F. The samples were fixed on a metal support and a double-surfaced carbon strip, coated with a thin layer of gold, and then viewed under 100–5000 magnification at an excitation voltage of 15 kV [24].

2.5. Adsorption Tests. The carotene removal was done following an adapted method from Silva et al. (2013). Especially, 50 g of crude palm oil is introduced into a 100 ml flask and heated to 75 and 95°C. Then, citric acid and the adsorbent are added, respectively, at 0.09% and 3.0% w/w, with respect to the mass of crude palm oil. The mixture is then submitted to high shear for 30 min at temperatures of 75°C and 95°C. The solutions are then filtered and the residual beta-carotene concentration was determined using a Corning spectrophotometer at 446 nm.

The quantity of β-carotene (mg/g) adsorbed was also calculated for clays and nZVI/activated clays using

$$Q_0 = \frac{C_0 - C_e}{m} V, \quad (1)$$

where m and V, respectively, are the mass of the adsorbents sample and the volume of the solution; C_0 (mg/L) and C_e (mg/L) are the initial and final (equilibrium) concentrations of the solute in solution.

The kinetic adsorption was carried out; 50 g of crude palm oil was introduced into a 100 ml flask and heated to 95°C. 0.09% w/w citric acid was added as a 30% w/w aqueous solution of a high shear mixture. 1.5% adsorbent was added and the resulting mixture was kept at 95°C with stirring for time ranging from 10 to 50 min. Then, the solutions were filtered, and the residual beta-carotene concentration was determined using a Corning spectrophotometer.

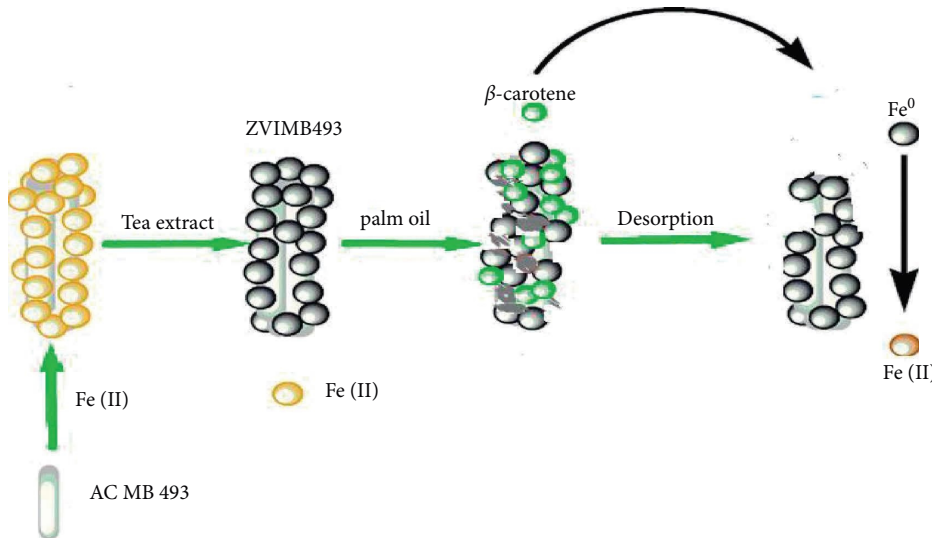

FIGURE 1: Schematic illustration of the immobilization of nanoscale zero valent iron particles on ACMB 493 and proposed mechanism for β-carotene desorption by ZVI MB 493.

2.6. Desorption Tests. The adsorption-desorption process was carried out in batch mode. 3 g of palm oil was dissolved in 100 ml citric acid. The solution thus obtained was mixed with 6 g of adsorbent in a 250 ml conical flask and stirred at room temperature for 2 h. After phase separation, the filtrate was taken for analysis. The regenerated adsorbent was then used for the 1st desorption process by adding 100 ml of hexane to a conical flask and stirring for 1 hour at room temperature. The adsorbent was filtered and the 1st filtrate was taken for analysis. The adsorption and desorption efficiency (%) was then calculated based on equations (2) and (3), respectively.

$$\%R = \frac{A_0 - A_e}{A_0} \cdot 100, \tag{2}$$

$$\%D = \frac{A_d}{A_0 - A_e} \cdot 100, \tag{3}$$

where $\%R$ is the adsorption efficiency; $\%D$ is the desorption efficiency; A_0 and A_e are the initial and equilibrium absorbance of the target component in the oil, respectively; and A_d is the target component absorbance in the oil after desorption.

2.7. Errors Estimations. This study allowed us to examine the nonlinear errors of the different kinetic models. In each case, the parameters χ^2, RMSE, and %APE have been evaluated. The smaller RMSE value indicates the best fit for the model. The RMSE can be defined as

$$\text{RMSE} = \sqrt{\frac{1}{N-2}\sum_{i=1}^{N}\left(q_{e,\exp} - q_{e,\text{cal}}\right)^2}. \tag{4}$$

The chi-square (χ^2) statistic [25] is given as

$$\chi^2 = \sum_{i=1}^{N}\frac{\left(q_{e,\exp} - q_{e,cal}\right)^2}{q_{e,cal}}. \tag{5}$$

The nonlinear χ^2 test is a statistical tool necessary for better fitting of an adsorption system, obtained by appreciating the sum of the squares differences between the experimental and calculated data, with each difference squared divided by its corresponding value (calculated from models). The small value χ^2 indicates its similarities, while a larger number represents variation in experimental data [26].

The correlation coefficients χ^2 show the fit between experimental data and kinetics equations, while the average percentage errors (% APE), calculated according to equation (6), indicated the fit between the experimental and predicted values of adsorption capacity used for plotting isotherm curves, where N is the number of experimental data [26].

$$\%\text{APE} = \frac{1}{N}\left[\sum_{i=1}^{N}\frac{\left(\left|q_{e,\exp} - q_{e,\text{cal}}\right|\right)}{q_{e,\exp}}\right] \times 100. \tag{6}$$

3. Results and Discussion

3.1. Characterization of Crude Clays, Activated Clays, and ZVI/Activated Clays. The infrared spectra were obtained for the crude clays and the adsorbents in a wavenumber range of 400–4000 cm^{-1} (Figure 2). All adsorbents presented a broad band in the region 3700–3500 cm^{-1} and are attributed to octahedral layer and hydroxyl stretching [20, 27]. The assignment of the band centered at 998 cm^{-1} is assigned to the vibratory deformation of the Al–OH–Al [28]. The bands at 908.9 and 827.9 cm^{-1} are attributed to Al–Al–OH and Al-Mg–OH, respectively. The bands at 592 cm^{-1} and 466 cm^{-1} are assigned to the Si–O–Al and Si–O–Si bending vibration, respectively [29, 30]. The band at 3052.62 cm^{-1} was ascribed to OH stretching vibration and the two bands at

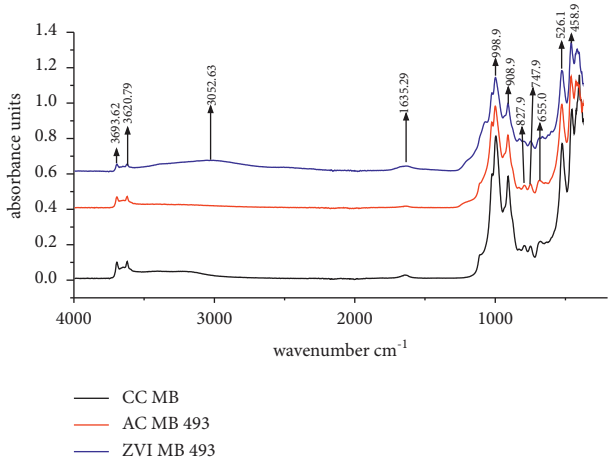

Figure 2: FTIR spectra of adsorbents crude clays CC MB acid-activated, AC MB 493, and ZVI MB 493 adsorbents.

1635.29 cm^{-1} and 1623 cm^{-1} to the OH bending vibration of surface-adsorbed water (Figure 1) which suggests the formation of ferric oxyhydroxide (FeOOH) layer on Fe^0 nanoparticles [31]. The broadband and intensive peak at 3244 cm^{-1} was assigned to the stretching of the O-H group of phenol [32, 33]. The peak at 2932 cm^{-1} is attributed to the symmetric and asymmetric C-H stretching vibration of flavonoids and phenolics, respectively. The peak at 1354 cm^{-1} indicated the O-H bend of polyphenol confirming the presence of an aromatic group [34]. The C-O stretching vibration at 1024 cm^{-1} was attributed to polyphenol compound [33] and adsorption band at 592 cm^{-1} was attributed to the Fe-O stretching vibration of iron oxides [35].

The morphologies of clays, CC MB, AC MB 493, and ZVI MB 493 were analyzed by SEM (Figure 3). We notice that Figure 3(a) shows the interstices in the form of lamellae interlaced with each other forming an agglomeration in several layers thus reducing the porosity of the material. Figure 3(b) allows us to highlight the effect of activation with H_2SO_4 acid. We observe a decrease in the agglomeration of the lamellae to the detriment of the fibers, thus promoting the formation of macroporosity. Figure 3(c) highlights the destruction of the agglomeration of interlaced fibers thus favoring the presence of small spherical balls symbolizing the presence of zero iron nanoparticles.

UV-vis spectral analysis allowed us to highlight the reduction of Fe^{3+} to nZVI. This was confirmed by the sudden change in the visible color of the reaction medium, serving as a preliminary indicator of the formation of nZVI. In the present study, an immediate change in the color of the solution from reddish-brown to black was observed after the addition of tea extract, indicating the rapid synthesis of nZVI (Figure 4). Fawzy et al. allowed us to conclude that the formation of the dark color of the synthesized nZVI is essentially due to the complexation of Fe^{3+} with the phenolic group in the plant extract as a metal-ligand interaction between Fe^0 and the polyphenolic compound via the C=O bond [36].

UV-vis spectra of the aqueous Fe^{3+} ions solution, tea extract, and synthesized nZVI (Figure 4) prove that the absorption spectrum of nZVI exhibited a maximum in the range of 216–300 nm, which is consistent with the characteristic absorption peak for metallic iron reported by [36]. These results are also in perfect harmony with the results published by [37, 38], where nZVI was synthesized from *Ricinus communis* with a peak of nZVI absorption in the wavelength range from 216 to 268 nm.

The chemical compositions of the sample CC MB are reported in Table 1. This table shows that the most dominant oxides are alumina and iron oxide. The two compounds constitute the basic structure of CC MB. They are followed by SiO_2, K_2O, CaO, and TiO_2. The other oxides (Mn_2O_3, V_2O_5, CuO, U_3O_8, As_2O_3, Ag_2O) have low contents.

The XRD patterns of the samples CC MB and ZVI MB 493 are given in Figure 5. They allow identifying the minerals contents in sample clays. The pattern of CC MB shows four intense pics. Two intense peaks of kaolinite ($d = 7.29$ Å and $d = 3.57$ Å), a peak of quartz ($d = 3.35$ Å), and a peak of iron ($d = 1.99$ Å). Other minerals are also found. The high content of Fe_2O_3 (32.54%) indicates that iron compounds are present in CC MB as gibbsite and goethite. In the pattern of ZVI MB 493, we notice that the crystallinity of kaolinite decreases with treatment, indicating the kaolin structure is destroyed. The peak at 2θ at 45.5° and 55.6° confirms the presence of Fe^0 [39, 40]. The peak is at 2θ at 45°, 65°, and 83° [41]; the peak at 2θ at 44° and 63° [39] confirms the presence of Fe^0. The peak at 2θ at 12°, and 27° designates the presence of FeO(OH) [41, 42]. The peak at 17° can be attributed to the presence of polyphenol/caffeine compounds [42]. A peak at 2θ at 29° and 35° is also observed which indicates the presence of Fe_3O_4 [35, 43].

3.2. Equilibrium Isotherms. The capacity of a CC MB, AC MB 493, and ZVI MB 493 can be described by equilibrium sorption isotherm, which is characterized by certain constants whose values express the surface properties and affinity of the CC MB, AC MB 493, and ZVI MB 493. The sorption isotherms were investigated using three equilibrium models, which are, namely, the Freundlich, Langmuir, and Temkin; these isotherm models were analyzed at 75°C and 95°C, respectively.

3.2.1. Langmuir Isotherm. A basic assumption of the Langmuir theory is that sorption takes place at specific homogeneous sites within the sorbent. This model can be written in linear form [44].

$$\frac{C_e}{Q_e} = \frac{1}{K_L Q_{\max}} + \frac{1}{Q_{\max}} C_e, \tag{7}$$

where Q_e is the equilibrium concentration of β-carotene on the adsorbent (mg·g^{-1}), C_e is the equilibrium concentration of β-carotene in the solution (mg·L^{-1}), $Q_{\max}$ is the adsorbent (mg·g^{-1}), and K_L is the monolayer adsorption capacity of the Langmuir adsorption constant (L·mg^{-1}) related with the free energy of adsorption. Figures 6 and 7 and Table 2 indicate

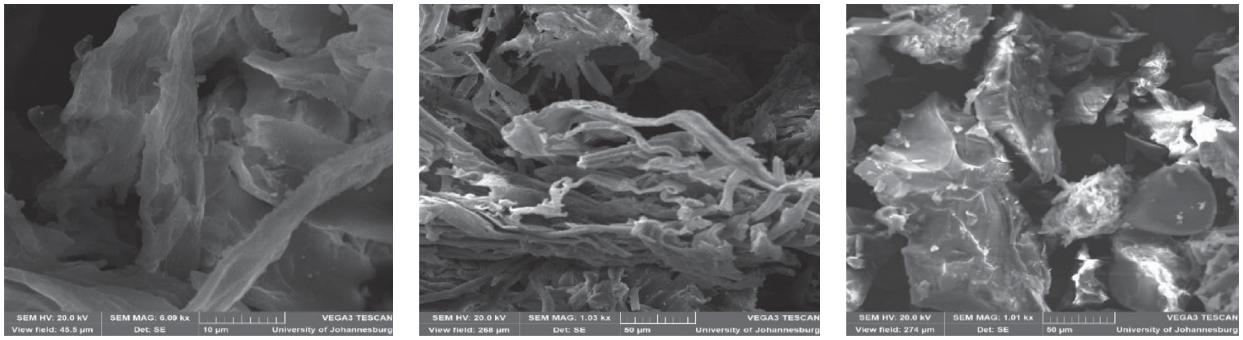

(a) (b) (c)

Figure 3: Scanning electron micrograph (SEM) of (a) CC MB, (b) AC MB 493, and (c) ZVI MB 493.

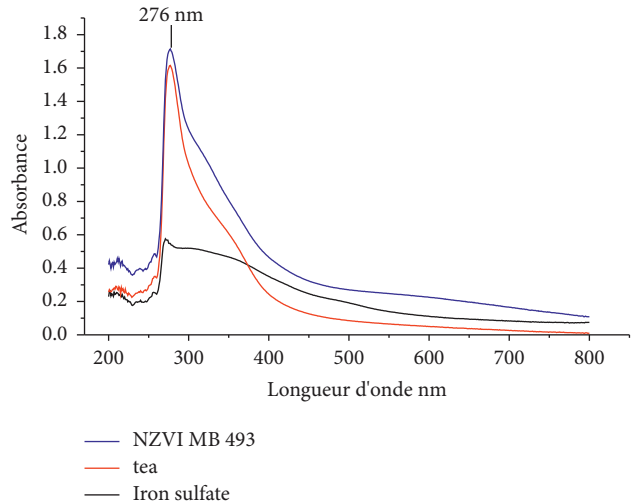

Figure 4: UV-visible absorption spectra of RC seed extract, an aqueous solution of Fe^{3+} ions, and synthesized nZVI.

Table 1: Chemical composition of CC MB.

No.	CC MB											
Oxide	Al_2O_3	Fe_2O_3	SiO_2	K_2O	CaO	TiO_2	Mn_2O_3	V_2O_5	CuO	U_3O_8	As_2O_3	Ag_2O
%wt	57.91	32.54	3.09	2.37	1.73	1.04	0.30	0.057	0.021	0.009	0.0029	0.0012

the linearity between the amount (mg) of β-carotene sorbed per unit mass (g) of CC MB, AC MB 493, and ZVI MB 493 with the concentration β-carotene remaining in solution (mg L^{-1}). The correlation coefficients (R^2) grouped in Table 2 indicates that the adsorption of the β-carotene onto CC MB, AC MB 493, and ZVI MB 493 fitted not well the Langmuir model. We also notice that the values of the Langmuir constant for the adsorption of beta-carotene are negative. This indicates the inadequacy of the isotherm model to explain the adsorption process since these constants are indicative of the surface binding energy and monolayer coverage [45]. The R_L values allow us to stratify the shape of the isotherm as follows: $R_L > 1$, unfavorable; $R_L = 1$, linear; $0 < R_L < 1$, favorable; and $R_L = 0$, irreversible. According to [44], R_L values between 0 and 1 indicate favorable adsorption. According to the values of R_L obtained in Table 2, the adsorption of β-carotene is not favorable.

Table 3 compares the maximum adsorption capacity of β-carotene (Q_{max}) with the literature. In view of the above, we can conclude that the Q_{max} values of AC MB 493 and ZVI MB 493 at 75°C and 95°C are greater than the values of the literature. We find that adsorption capacity increases with temperature and ZVI MB 493 has higher adsorption capacity than AC MB 493 and CC MB.

3.2.2. Freundlich Isotherm. The Freundlich model assumes active sites of different energy and a heterogeneous adsorption surface. The Freundlich model can be written in linear form [44, 50].

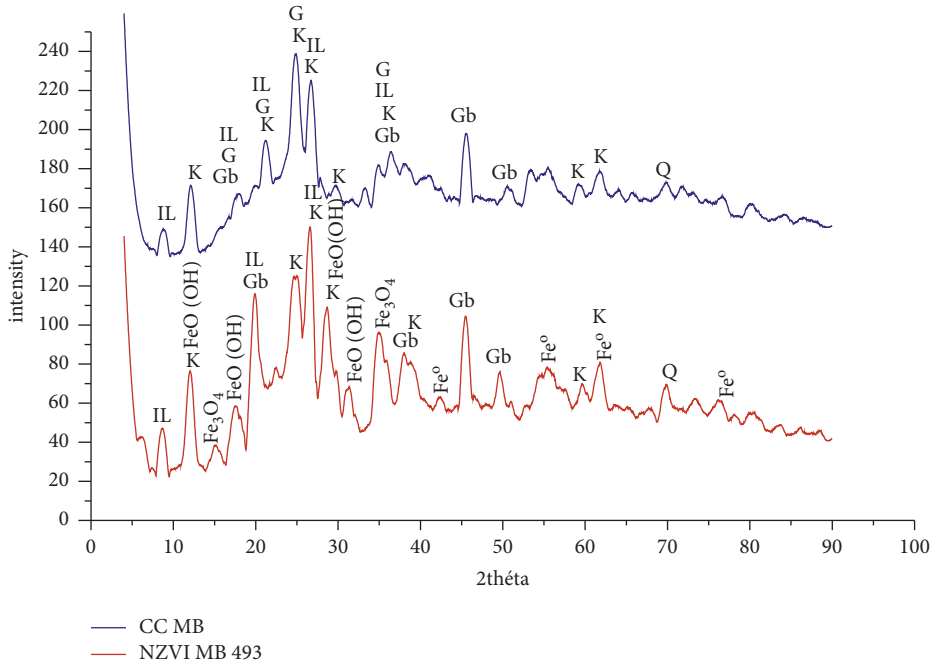

Figure 5: XRD patterns of CC MB and ZVI MB 493.

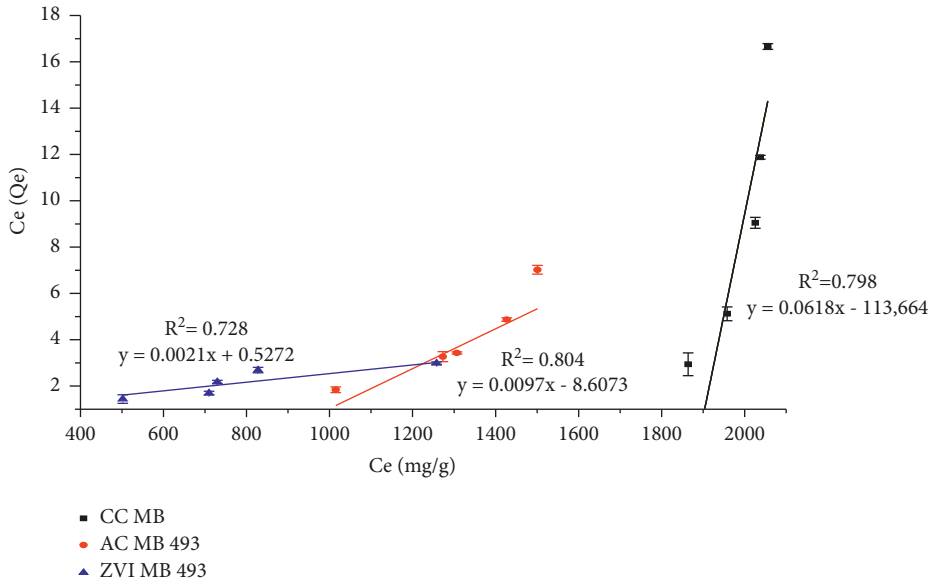

Figure 6: Langmuir adsorption isotherm for removal of β-carotene onto CC MB, AC MB 493, and ZVI MB 493 at 75°C.

$$\log\left(\frac{x}{m}\right) = \log K_F + \frac{1}{n}\log C_e, \tag{8}$$

where K_F is the constant derived from the adsorption capacity and $1/n$ is a parameter relating to the adsorption intensity, which is a function of the heterogeneity of the material (Figures 8 and 9 and Table 2). The value of K_F increases with an increase in temperature indicating the good adsorption capacity of adsorbents. The values of n indicate that the type of adsorption is favorable in the range of 2–10, moderate in the range of 1-2, and poor if $n < 1$ [51]. We observe an increase in n values with an increase in the temperature. Table 2 shows that all values of n at 75°C and 90°C were less than unity, indicating that adsorption of the β-carotene is weak. R^2 values are greater than for all adsorbents. These results show that the equilibrium adsorption data were well fitted by Freundlich isotherm at 75°C and 95°C compared to the Langmuir isotherms based on R^2.

3.2.3. Temkin Isotherm. The Temkin isotherm highlights adsorbent-adsorbate interactions. In this equation, it is assumed that, because of these interactions and ignoring very low and very large concentration values, the heat of

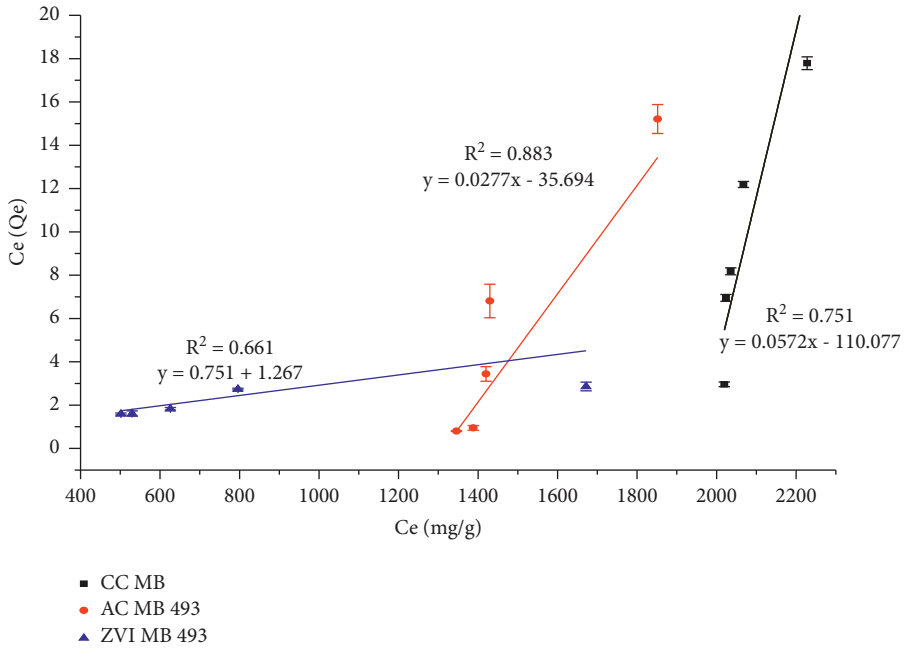

Figure 7: Langmuir adsorption isotherm for removal of β-carotene onto CC MB, AC MB 493, and ZVI MB 493 at 95°C.

Table 2: Freundlich, Langmuir, and Temkin constants for the adsorption of β-carotene onto CC MB, AC MB 493, and ZVI MB 493 at 75°C and 95°C.

Adsorbents	Langmuir			Freundlich			Temkin		
	K_L (L mg^{-1})	Q_{max}	R^2	K_F	n	R^2	A_T (L g^{-1})	b_T (KJ mol^{-1})	R^2
				75°C					
CC MB	$-5.43.10^{-4}$	16.180	0.798	$2.05.10^{-21}$	0.143	0.972	$5.405.10^{-4}$	4.333	0.656
AC MB 493	$-2.045.10^{-3}$	134.601	0.804	$2.52.10^{-10}$	0.253	0.967	$1.10.10^{-3}$	1.305	0.787
ZVI MB493	3.32×10^{-3}	151.520	0.728	$2.29.10^{-3}$	0.559	0.975	$2.205.10^{-3}$	0.803	0.933
				95°C					
CC MB	$-5.24.10^{-4}$	17.330	0.751	$8.051.10^{-15}$	0.205	0.973	$5.075.10^{-4}$	1.512	0.840
AC MB 493	$-7.54.10^{-4}$	144.928	0.883	$7.98.10^{-4}$	0.539	0.984	$2.978.10^{-3}$	0.751	0.867
ZVI MB 493	$-2.1.10^{-2}$	256.410	0.661	$9.11.10^{-4}$	0.508	0.980	$2.504.10^{-3}$	0.962	0.977

Table 3: Comparative adsorption capacity Q_{max} of β-carotene at 75°C and 95°C.

Adsorbents	Q_{max} (mg/g)	Solvent	Reference
75°C			
AAB	79.55	Cyclohexane	[46]
AAB	92.59	Xylene	[47]
CC MB	16.180		
AC MB 493	134.601	Citric acid	This study
ZVIMB 493	251.520		
95°C			
Tonsil OPP210 FF	33	Citric acid	[26]
Earth activated	64.40	Hexane	[48]
NBE	29.22	Ethanol/ethylether	[49]
AAB	107.53	Xylene	[47]
CC MB	17.330		
AC MB 493	144.928	Citric acid	This study
ZVIMB 493	256.410		

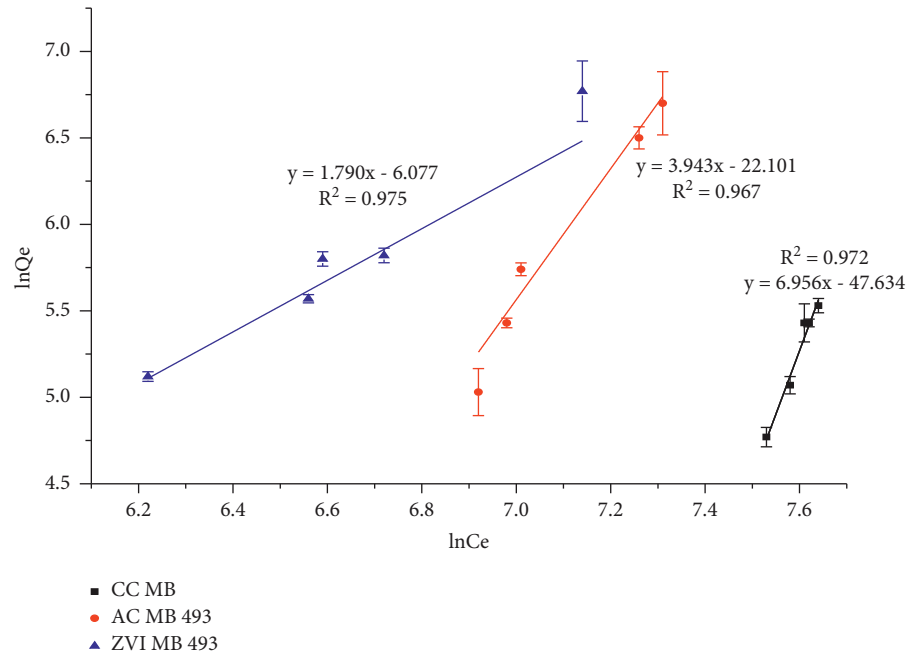

Figure 8: Freundlich adsorption isotherm for the removal of β-carotene onto CC MB, AC MB 493, and ZVI MB 493 at 75°C.

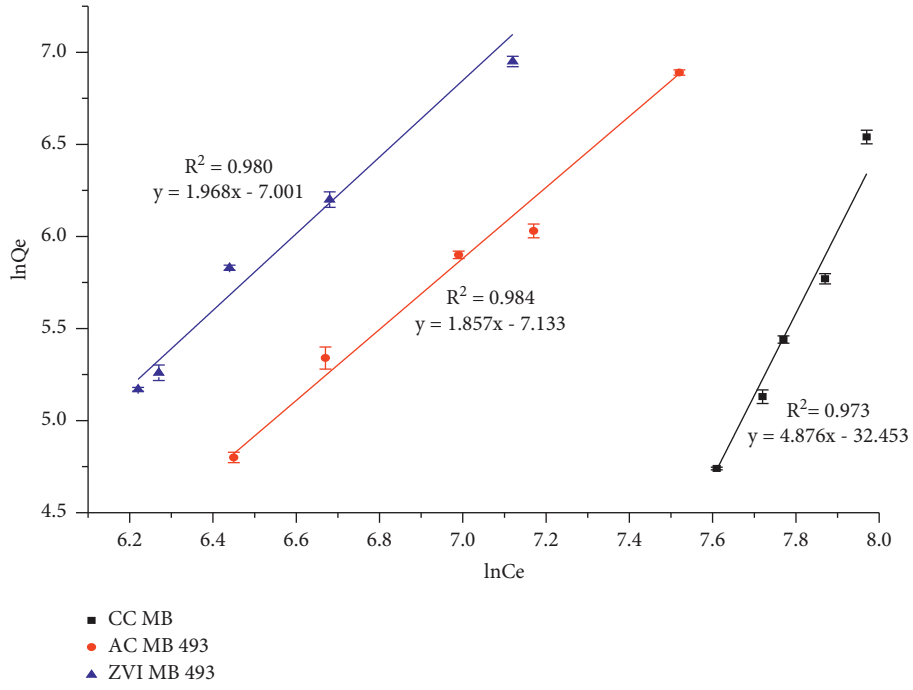

Figure 9: Freundlich adsorption isotherm for the removal of β-carotene onto CC MB, AC MB 493, and ZVI MB 493 at 95°C.

adsorption of all molecules in the layer would decrease linearly with the coverage [52]. Temkin's linear model is written as

$$Qe = B \ln AT + B \ln Ce, \quad (9)$$

where A_T is the equilibrium binding constant corresponding to the maximum binding energy, $B = R/b_T$, b_T (J mol^{-1}) is the Temkin constant related to the heat of adsorption, R (8.314 Jmol^{-1}·K^{-1}) is the universal gas constant, and T (K) is the solution temperature.

The values of the constants thus obtained from the Temkin isotherm (Figures 10 and 11 and Table 2) were, respectively, as follows: $A_T = 5.405.10^{-4}$ L/g, $b_T = 4.333$ kJ·mol^{-1} for CC MB, $A_T = 10^{-3}$ L/g, $b_T = 1.305$ kJ·mol^{-1} for AC MB 493, and $A_T = 10^{-3}$ L/g, $b_T = 0.803$ kJ·mol^{-1} for ZVI MB 493 at 75°C; and

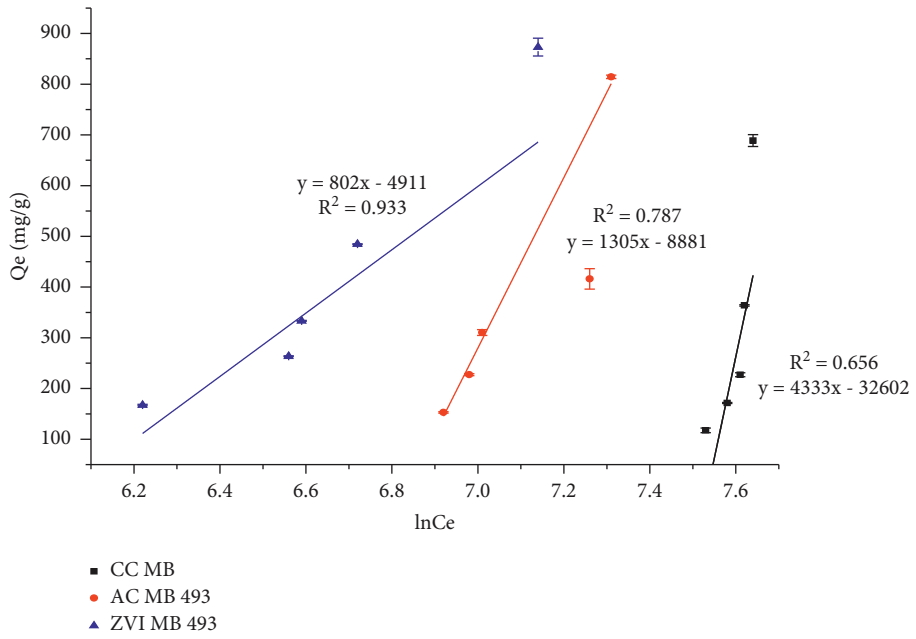

Figure 10: Temkin adsorption isotherm for removal of β-carotene onto CC MB, AC MB 493, and ZVI MB 493 at 75°C.

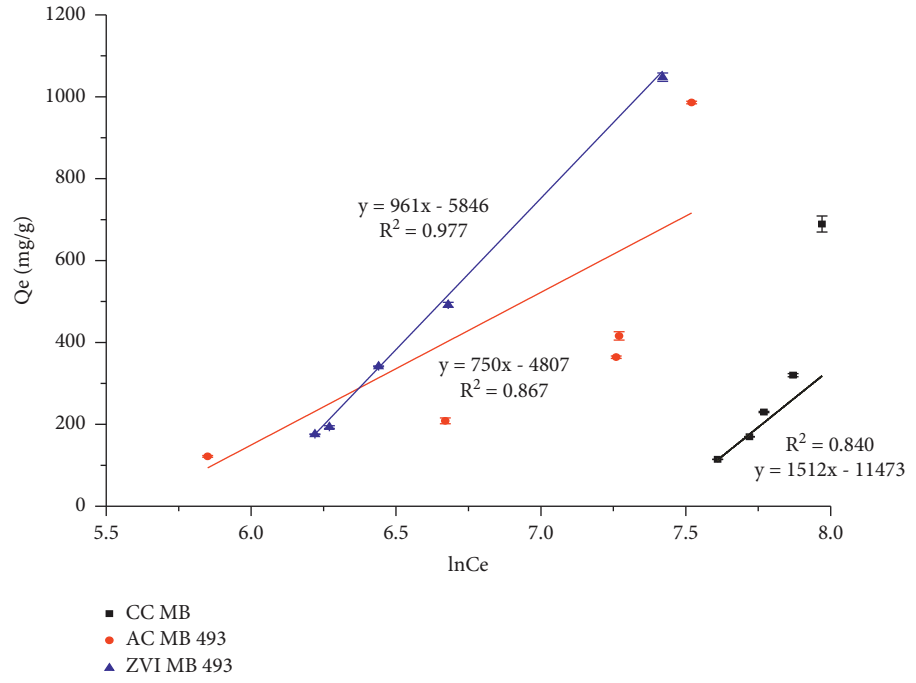

Figure 11: Temkin adsorption isotherm for removal of β-carotene onto CC MB, AC MB 493, and ZVI MB 493 at 95°C.

$A_T = 5.075.10^{-4}$ L/g, $b_T = 1.512$ kJ·mol^{-1} for CC MB, $A_T = 2.978.10^{-3}$ L/g, $b_T = 0.382$ kJ·mol^{-1} for AC MB 493, and $A_T = 2.504.10^{-3}$ L/g, $b_T = 0.751$ kJ·mol^{-1} for ZVI MB 493 at 95°C, indicating that the adsorption isotherm of Temkin for removal of β-carotene onto CC MB, AC MB 493, and ZVI MB 493 occurred via physisorption. The constant b_T in Temkin isotherms is less than 20 kJ·mol^{-1}, so the mechanism involved is physical adsorption [53]. In the physisorption process, the adsorbates adhere to the adsorbent through weak Van Der Waals interactions, and thus, this process is associated with relatively low adsorption energies [54].

3.3. Adsorption Kinetics. The kinetic study is an adsorption process that provides information on the adsorption mechanism and the mode of transfer between the two solid

and liquid phases. In this study, three kinetic models have been used to elucidate the mechanism of β-carotene adsorption at 95°C onto the surface of CC MB, AC MB 493, and ZVI MB 493 such as the pseudo-first-order kinetic model, the pseudo-second-order kinetic model, and the intraparticle diffusion model.

3.3.1. First-Order and Pseudo-Second-Order Kinetic Models. The mechanism of the adsorption process depends on the physical and chemical characteristics of the adsorbent and adsorbate. To investigate the kinetics adsorption of β-carotene, the Lagergren-first-order and Ho's pseudo-second-order kinetic models were used.

The pseudo-first-order rate equation was proposed by Lagergren and is widely used for the adsorption of liquid/solid systems [55]. The linear form of Lagergren equation is generally expressed as

$$\log(q_e - q_t) = -\log q_e - \frac{k_1 t}{2.303}, \quad (10)$$

where k_1 (min^{-1}) is the pseudo-first-order rate constant at equilibrium. q_e and q_t are the adsorption uptake of adsorbate at equilibrium and at time t(min), respectively. The pseudo-first-order plots for β-carotene are shown in Figure 12.

The pseudo-second-order model [44, 56] suggests that both the number of adsorption sites on the material surface and the concentration of adsorbate ions in the liquid phase determine the rate. The linearized form of the model is

$$\left(\frac{t}{q_t}\right) = \left(\frac{t}{q_e}\right) + \left[\left(\frac{1}{k_2 q_e^2}\right)\right], \quad (11)$$

where $h = k_2 q_e^2$ and k_2 are the initial and overall rate constants for adsorption which can be calculated from the slope and intercept of plot t/q_t vs. t. The linear forms of the pseudo-second-order model are given in Figure 13.

The kinetic parameters of adsorption of β-carotene onto CC MB, AC MB 493, and ZVI MB 493 are found in Table 4. These parameters were obtained from the slope and intercept of linear plots of the kinetics equations. The values of the correlation coefficient (R^2) obtained for the pseudo-first-order kinetic model and the intraparticle diffusion model are all less than 0.789 and those of the pseudo-second-order model are greater than 0.965. In addition, the calculated Q_e values obtained from the linear plots agree with the experimental values and increase significantly with the activation and impregnation of the adsorbents with acid and zero iron nanoparticles. The pseudo-second-order model is suitable to explain the adsorption of β-carotene onto CC MB, AC MB 493, and ZVI MB 493.

3.3.2. Intraparticle Diffusion Model. The adsorbed solute particles diffuse into the pores on the surface of the adsorbent and form a bond, which could be the rate-determining step [57]. The Weber and Morris intraparticle diffusion model is given by the following equation:

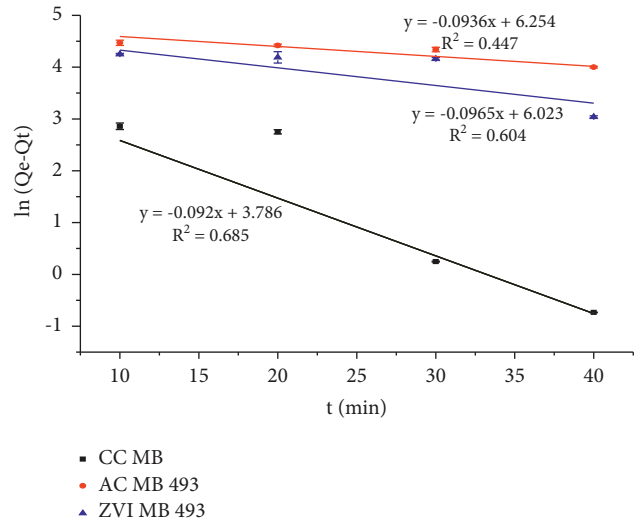

Figure 12: Adsorption curves of the pseudo-first-order model onto CC MB, AC MB 493, and ZVI MB 493 at 95°C.

$$q = f\left(\frac{D_t}{r_p^2}\right)^{1/2} = k_w t^{1/2}, \quad (12)$$

where k_w (mg $\text{g}^{-1}\cdot\text{min}^{-1/2}$) is the rate constant for intraparticle diffusion; k_w can be found from the slope of plot q_t vs $t^{1/2}$. For the intraparticle diffusion model, the straight line must pass through the origin and the intercept value provides an idea of the deviation from the intraparticle diffusion model or the contribution of the film diffusion mechanism [44]. In the case of the Morris–Weber equation (Figure 14), the straight lines of β-carotene do not pass through the origin, demonstrating that intraparticle diffusion is not the only kinetically controlling step, but other mechanisms are also involved in the rate-determining step.

3.4. Reusability. Figure 15 shows that the result of the extraction of β-carotene by our different adsorbents varies from 40.5 to 70.3%, unlike the percentage of adsorption which varies from 60.8 to 93.6%. After regeneration of our various adsorbents, we find that the percentage of beta-carotene adsorption decreases. This loss in adsorption capacity has been attributed to the incomplete removal of b-carotene molecules from within the clay structure during regeneration, which hinders the availability of active sites in the regenerated adsorbent for the next adsorption bleaching cycle [58].

3.5. Errors Analysis for Kinetics Models. A comparative study between linear and nonlinear approaches of each pseudo-first-order, pseudo-second-order, and intraparticle diffusion kinetic model was also performed to select the most appropriate shape. The linear and nonlinear form of the second-order kinetic model was found to be the linear and nonlinear forms that best describe the experimental data

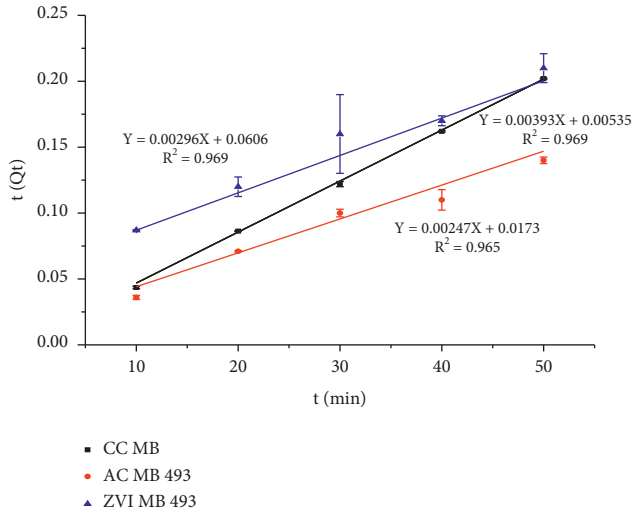

Figure 13: Adsorption curves of the pseudo-second-order model onto CC MB, AC MB 493, and ZVI MB 493 at 95°C.

Table 4: Kinetics parameters of adsorption of β-carotene onto CC MB, AC MB 493, and ZVI MB 493.

Adsorbents	Pseudo-first-order				Pseudo-second-order			Intraparticle diffusion		
	Q_{exp} (mg g^{-1})	K_1 (min^{-1})	Q_{ecal} (mg g^{-1})	R^2	K_2 (mg g^{-1}.min)	$Q_{e\ cal}$ (mg g^{-1})	R^2	k_{int} (mg g^{-1}·min^{-1})	$Q_{e\ cal}$ (mg·g^{-1})	R^2
CC MB	230.103	0.133	99.685	0.684	2.82×10^{-3}	254.45	0.969	5.243	249.82	0.789
AC MB 493	414.012	0.015	107.776	0.447	9.37×10^{-5}	404.850	0.965	37.186	401.620	0.681
ZVI MB 493	309.532	0.037	124.592	0.604	1.49×10^{-4}	337.830	0.969	20.175	336.725	0.653

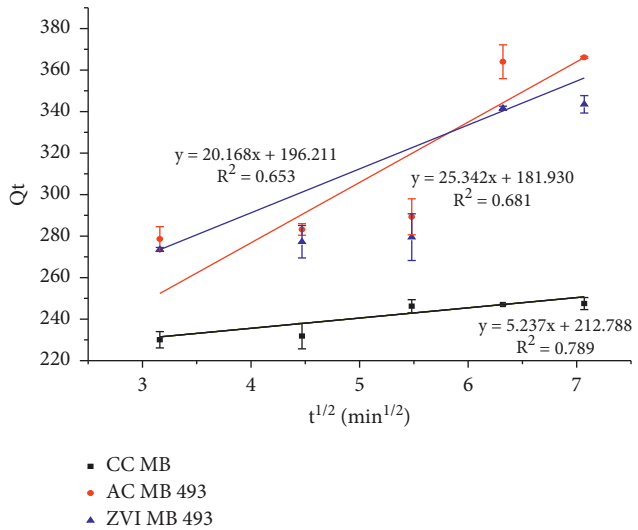

Figure 14: Adsorption curves of the intraparticle diffusion model onto CC MB, AC MB 493, and ZVI ACMB 493 at 95°C.

with regard to the correlation coefficients R^2 and small error functions (χ^2, RMSE and %APE) (Table 5).

4. Adsorption Thermodynamics

Thermodynamic parameters explain the effect of temperature on adsorption. They predict the strength of the bonds between the adsorbent and the adsorbate. These parameters are enthalpy ΔH°, entropy ΔS°, and free enthalpy ΔG°. The equations used are as follows:

$$\ln k_d = -\frac{\Delta H^\circ}{RT} + \frac{\Delta S^\circ}{R}, \tag{13}$$

where ΔH° is the standard enthalpy, ΔS° is the standard entropy, ΔG° is the Gibbs free enthalpy, K_d is the distribution coefficient, and $\Delta G^\circ = \Delta H - T\Delta S^\circ$.

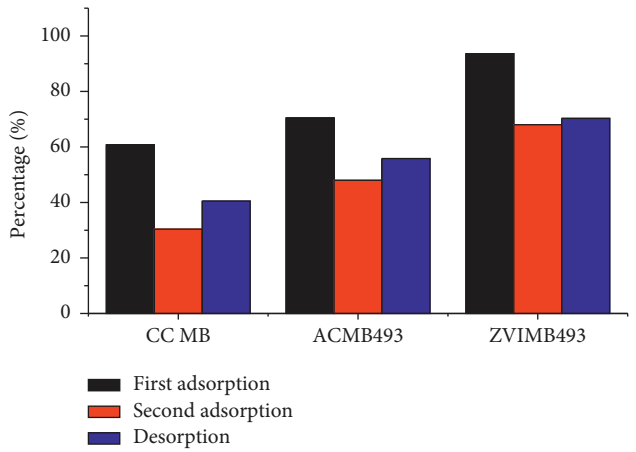

Figure 15: Effect of adsorption efficiency (%), desorption efficiency (%), and extraction process on percentage of β-carotene extracted.

Table 5: The error functions parameters of β-carotene adsorption onto CC MB, AC MB 493, and ZVI MB 493 at 95°C.

Adsorbents	Pseudo-first-order				Pseudo-second-order				Diffusion intraparticle			
	R^2	χ^2	RMSE	%APE	R^2	χ^2	RMSE	%APE	R^2	χ^2	RMSE	%APE
CC MB	0.902	170.63	130.42	56.68	0.999	2.70	26.31	6.60	0.842	1.56	19.72	8.57
AC MB 493	0.824	870.16	306.23	65.92	0.975	0.49	14.00	3.38	0.831	0.38	12.40	2.99
ZVI MB 493	0.661	274.43	184.91	58.89	0.977	1.70	23.83	7.70	0.740	2.20	27.20	8.79

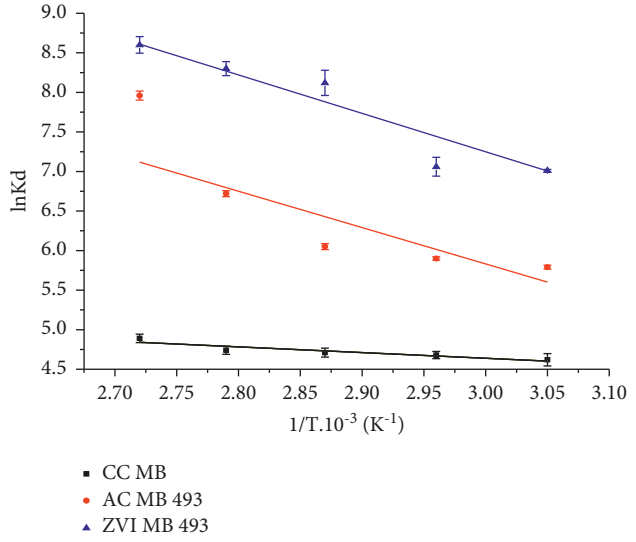

Figure 16: Adsorption isosteres used to determine the isosteric heat of carotenes onto CC MB, AC MB 493, and ZVI MB 493 at 95°C.

The plot of the $\ln k_d$ curve as a function of the inverse of the temperature ($1/T$), as in Figure 16, allowed us to deduce the values of ΔH°, ΔS°, and ΔG° from Table 6. In view of the above, the values of ΔH° are positives, which showed that the biosorption reaction is endothermic due to the increase in biosorption upon a successive increase in the temperature. The heat released during physical adsorption is of the order of 2.1–20.9 kJ·mol^{-1}, while that which developed during chemical sorption is of the order of 80–200 kJ·mol^{-1}. Therefore, as shown in Table 6, it is inferred that the adsorption of β-carotene on CC MB is physisorption, while the adsorption of β-carotene onto AC MB 493 and ZVI MB 493 can be attributed to a physicochemical adsorption process rather than a pure physical or chemical adsorption process [58, 59]. Because the values of ΔH° range between 20.9 and 200 kJ·mol^{-1}. The positive values of ΔS indicate enhanced randomization at the solid-solution interface

Table 6: Equilibrium constants, standard Gibbs free energy, enthalpy, and entropy of carotenes adsorption from crude palm oil onto CC MB, AC MB 493, and ZVI MB 493 at 95°C.

	ΔG° (kJ mol^{-1})					ΔH° (kJ mol^{-1})	ΔS° (kJ mol^{-1})
Temperature (K)	328	338	348	358	368		
CC MB	−12.567	−13.130	−13.693	−14.256	−14.819	5.899	0.0563
AC MB 493	−20,644	−22.824	−25.004	−27.184	−29.364	50.860	0.213
ZVI MB 493	−18.990	−20.750	−22.510	−24.270	−26.030	38.768	0.176

β-carotene adsorption on the active sites of the CC MB, AC MB 493, and ZVI MB 493. Negative values of ΔG° also reveal adsorption by adsorbents is thermodynamically spontaneous.

5. Conclusion

The effectiveness of the CC MB, AC MB 493, and ZVI MB 493 for the uptake of β-carotene from an aqueous solution was evaluated. The experimental results showed that the CC MB, AC MB 493, and ZVI MB 493 could effectively remove β-carotene of palm oil. Adsorbent characterization showed that alumina iron oxides and silica, due to their high content, constitute the basic structure of the studied clay. The adsorption process is a function of the adsorbate-adsorbent contact time and temperature. The adsorption of β-carotene is also a function of the physicochemical adsorption process, the influence of the mass transfer of oil at the adsorbent-oil interface, and the heterogeneity of the adsorption sites on the clay and the nature of the adsorbate. The adsorption of β-carotene onto CC MB, AC MB 493, and ZVI MB 493 can be attributed to a physisorption adsorption process. It was also found that pore diffusion played an important role in adsorption. The Freundlich isotherm showed a better fit than the Langmuir and Temkin isotherms, thus indicating the applicability of the heterogeneity of β-carotene on CC MB, AC MB 493, and ZVI MB 493, while the isotherm from Temkin is at 75°C. Thermodynamic analysis shows that the adsorption process was spontaneous. The FTIR spectra and the SEM images of CC MB, AC MB 493, and ZVI MB 493 showed that the structure was modified by treatment.

Data Availability

The data used to support the findings of this study are available from the corresponding author upon request.

Conflicts of Interest

The authors declare that they have no conflicts of interest.

References

[1] A. J. Hambly, S. Jeroen, V. Duijneveldt, and P. J. Gates, "Identification of ß-carotene oxidation products produced by bleaching clay using UPLC-ESI-MS/MS," *Food Chemistry*, vol. 353, no. 2921, Article ID 129455, 2021.

[2] J. A. A. Ribeiro, E. S. Almeida, B. A. Neto, P. V. Abdelnur, and S. Monteiro, "Identification of carotenoid isomers in crude and bleached palm oils by mass spectrometry," *LWT--Food Science and Technology*, vol. 89, pp. 631–637, 2018.

[3] B. Gil, M. Kim, J. H. Kim, and S. H. Yoon, "Comparative study of soybean oil refining using rice hull silicate and commercial adsorbents," *Food Science and Biotechnology*, vol. 23, no. 4, pp. 1025–1028, 2014.

[4] K. S. d. Araújo, S. M. S. e. Silva, L. D. d. Santos, C. B. Malafaia, and M. O. Barbosa, "A preliminary study of the physicochemical properties and fatty acid profile of five palm oil genotypes cultivated in Northeast of Brazil," *Journal of Environmental Analysis and Progress*, vol. 04, pp. 251–256, 2019.

[5] C. A. Van Loo-Bouwman, T. H. J. Naber, and G. Schaafsma, "A review of vitamin A equivalency of β-carotene in various food matrices for human consumption," *British Journal of Nutrition*, vol. 111, no. 12, pp. 2153–2166, 2014.

[6] F. Nabi, M. A. Arain, N. Rajput et al., "Health benefits of carotenoids and potential application in poultry industry: a review," *Journal of Animal Physiology and Animal Nutrition*, vol. 104, no. 6, pp. 1809–1818, 2020.

[7] K. Pabari, S. Pithva, C. Kothari et al., "Evaluation of probiotic properties and prebiotic utilization potential of weissella paramesenteroides isolated from fruits," *Probiotics and Antimicrobial Proteins*, vol. 12, no. 3, pp. 1126–1138, 2020.

[8] J. K. Rutz, C. D. Borges, R. C. Zambiazi, M. M. Crizel-Cardozo, L. S. Kuck, and C. P. Noreña, "Microencapsulation of palm oil by complex coacervation for application in food systems," *Food Chemistry*, vol. 220, no. 59–66, pp. 59–66, 2017.

[9] A. J. Dijkstra, *Edible Oil Processing from a Patent Perspective Chapter*, pp. 173–198, Bleaching Springer, New York, NY, USA, 2013.

[10] C. Vaisali, S. Charanyaa, P. D. Belur, and I. Regupathi, "Refining of edible oils: a critical appraisal of current and potential technologies," *International Journal of Food Science and Technology*, vol. 50, no. 1, pp. 13–23, 2014.

[11] S. P. Santoso, A. E. Angkawijaya, M. Yuliana et al., "Saponin-intercalated organoclays for adsorptive removal of β-carotene: equilibrium, reusability, and phytotoxicity assessment," *Journal of the Taiwan Institute of Chemical Engineers*, vol. 117, pp. 198–208, 2020.

[12] F. Kreps, L. Vrbikova, and S. Schmidt, "Influence of industrial physical refining on tocopherol, chlorophyll and beta-carotene content in sunflower and rapeseed oil," *European Journal of Lipid Science and Technology*, vol. 116, no. 11, pp. 1572–1582, 2014.

[13] F. Marrakchi, K. Kriaa, B. Hadrich, and N. Kechaou, "Experimental investigation of processing parameters and effects of degumming, neutralization and bleaching on lampante virgin olive oils quality," *Food and Bioproducts Processing*, vol. 94, pp. 124–135, 2015.

[14] S. M. Silva, K. A. Sampaio, R. Ceriani et al., "Effect of type of bleaching earth on the final color of refined palm oil," *LWT—Food Science and Technology*, vol. 59, no. 2, pp. 1258–1264, 2014.

[15] D. Pranowo, B. S. D. Dewanti, H. Fatimah, and H. Y. Setyawan, "Optimization of regeneration process of spent bleaching earth," *IOP Conference Series: Earth and Environmental Science*, vol. 524, no. 1, p. 012011, 2020.

[16] A. Boukerroui, L. Belhocine, and S. Ferroudj, "Regeneration and reuse waste from an edible oil refinery," *Environmental Science and Pollution Research*, vol. 25, no. 19, pp. 18278–18285, 2017.

[17] A. Aishat, S. Olalekan, A. O. Arinkoola, and J. Omolola, "Effect of activation on clays and carbonaceous materials in vegetable oil bleaching: state of art review," *BJAST*, vol. 5, no. 2, pp. 130–141, 2015.

[18] V. Plata, Ó. Rojas, and P. Gauthier-Maradei, "Improvement of palm oil biodiesel filterability by treatment with reactivated spent bleaching earths," *Fuel*, vol. 260, Article ID 116198, 2020.

[19] L. L. Aung, E. Tertre, P. Suksabye, N. Worasith, and P. Thiravetyan, "Effect of alumina content and surface area of acid-activated kaolin on bleaching of rice bran oil," *Journal of the American Oil Chemists Society*, vol. 92, no. 2, pp. 295–304, 2015.

[20] A. K. Panda, B. G. Mishra, D. K. Mishra, and R. K. Singh, "Effect of sulphuric acid treatment on the physico-chemical characteristics of kaolin clay," *Colloids and Surfaces A: Physicochemical and Engineering Aspects*, vol. 363, no. 1–3, pp. 98–104, 2010.

[21] N. Worasith, B. A. Goodman, N. Jeyashoke, and P. Thiravetyan, "Decolorization of rice bran oil using modified kaolin," *Journal of the American Oil Chemists Society*, vol. 88, no. 12, pp. 2005–2014, 2011.

[22] M. Auffan, H. J. Shipley, S. Yean, and A. T. Kan, *Environmental Nanotechnology*, McGraw-Hill, New York, NY, USA, 2007.

[23] G. E. Hoag, J. B. Collins, J. L. Holcomb, J. R. Hoag, M. N. Nadagouda, and R. S. Varma, "Degradation of bromothymol blue by "greener" nano-scale zero-valent iron synthesized using tea polyphenols," *Journal of Materials Chemistry*, vol. 19, no. 45, p. 8671, 2009.

[24] J. K. Rutz, C. D. Borges, R. C. Zambiazi, C. G. da Rosa, and M. M. da Silva, "Elaboration of microparticles of carotenoids from natural and synthetic sources for applications in food," *Food Chemistry*, vol. 202, pp. 324–333, 2016.

[25] S. M. Silva, K. A. Sampaio, R. Ceriani et al., "Adsorption of carotenes andphosphorus from palm oil onto acid activated bleaching earth: equilibrium, kinetics and thermodynamics," *Journal of Food Engineering*, vol. 118, no. 4, pp. 341–349, 2013.

[26] M. Hadi, M. R. Samarghandi, and G. McKay, "Equilibrium two-parameter isotherms of acid dyes sorption by activated carbons: study of residual errors," *Chemical Engineering Journal*, vol. 160, no. 2, pp. 408–416, 2010.

[27] C. Akmil-Basar, G. Durmaz, I. Karabulut, and Y. Önal, "ß-carotene rejection mechanism from organic medium by using activated carbon produced fromwaste biomass apricot," *Particulate Science and Technology*, vol. 35, pp. 1–9, 2016.

[28] M. A. Asghar, E. Zahir, S. M. Shahid et al., "LWT, iron, copper and silver nanoparticles green synthesis using green and black tea leaves extracts and evaluation of antibacterial, antifungal and aflatoxin B_1 adsorption activity," *Food Science and Technology*, vol. 90, pp. 98–107, 2018.

[29] Y. Dehmani, A. Ed-Dra, Z. Omar et al., *Chemical characterization and adsorption of oil mill wastewater on Moroccan clay in order to be used in the agricultural field Heliyon*, vol. 6, Article ID e03164, 2020.

[30] W. Gao, S. Zhao, H. Wu, W. Deligeer, and S. Asuha, "Direct acid activation of kaolinite and its effects on the adsorption of methylene blue," *Applied Clay Science*, vol. 126, pp. 98–106, 2016.

[31] I. FernandoMac-as-Quiroga, "Gloria inés giraldo-gómez, and nancy roc-o sanabria-gonzález characterization of Colombian clay and its potential use as adsorbent," *The Scientific World Journal*, vol. 2018, p. 11, Article ID 5969178, 2018.

[32] X. Jin, Z. Chen, R. Zhou, and Z. Chen, "Synthesis of kaolin supported nanoscale zero-valent iron and its degradation mechanism of direct fast black G in aqueous solution," *Materials Research Bulletin*, vol. 61, pp. 433–438, 2015.

[33] M. Iqbal, A. Saeed, and S. I. Zafar, "FTIR spectrophotometry, kinetics and adsorption isotherm modelling, ion exchange and EDX analysis for understanding the mechanism of Cd^{2+} and Pb^{2+} removal by mango peel waste," *Journal of Hazardous Materials*, vol. 164, no. 1, pp. 161–171, 2009.

[34] D. Cao, X. Jin, L. Gan, T. Wang, and Z. Chen, "Removal of phosphate using iron oxide nanoparticles synthesized by eucalyptus leaf extract in the presence of CTAB surfactant," *Chemosphere*, vol. 159, pp. 23–31, 2016.

[35] C. P. Devatha, A. K. Thalla, and S. Y. Katte, "Green synthesis of iron nanoparticles using different leaf extracts for treatment of domestic waste water," *Journal of Cleaner Production*, vol. 139, pp. 1425–1435, 2016.

[36] R. Ahmed, M. Tariq, I. Ali et al., "Novel electrospun chitosan/polyvinyl alcohol/zinc oxide nanofibrous mats with antibacterial and antioxidant properties for diabetic wound healing," *International Journal of Biological Macromolecules*, vol. 120, pp. 385–393, 2018.

[37] L. Huang, X. Weng, Z. Chen, M. Megharaj, and R. Naidu, "Green synthesis of iron nanoparticles by various tea extracts: comparative study of the reactivity," *Spectrochimica Acta Part A: Molecular and Biomolecular Spectroscopy*, vol. 130, no. 15, pp. 295–301, 2014.

[38] R. Singh, V. Misra, and R. P. Singh, "Synthesis, characterization and role of zero-valent iron nanoparticle in removal of hexavalent chromium from chromium-spiked soil," *Journal of Nanoparticle Research*, vol. 13, no. 9, pp. 4063–4073, 2011.

[39] A. S. E. Fawzy and M. E. El-Khouly, "Green synthesis of nano-zero-valent iron using Ricinus Communis seeds extract: characterization and application in the treatment of methylene blue-polluted water ahmed M. Abdelfatah, manal," *ACS Omega*, vol. 6, pp. 25397–25411, 2021.

[40] M. Ahmad, A. R. A. Usman, M. I. Rafique, and M. I. Al-Wabel, "Engineered biochar composites with zeolite, silica, and nano-zerovalent iron for the efficient scavenging of chlortetracycline from aqueous solutions," *Environmental Science and Pollution Research*, vol. 26, no. 15, pp. 15136–15152, 2019.

[41] B. Kakavandi, A. Esrafili, A. Mohseni-Bandpi, A. Jonidi Jafari, and R. Rezaei Kalantary, "Magnetic Fe3O4@C nanoparticles as adsorbents for removal of amoxicillin from aqueous solution," *Water Science and Technology*, vol. 69, no. 1, pp. 147–155, 2014.

[42] S. R. Kanel, B. Manning, L. Charlet, and H. Choi, "Removal of arsenic(III) from groundwater by nanoscale zero-valent iron," *Environmental Science and Technology*, vol. 39, no. 5, pp. 1291–1298, 2005.

[43] T. Shahwan, S. Abu Sirriah, M. Nairat et al., "Green synthesis of iron nanoparticles and their application as a Fenton-like catalyst for the degradation of aqueous cationic and anionic dyes," *Chemical Engineering Journal*, vol. 172, no. 1, pp. 258–266, 2011.

[44] C. M. Kede, P. P. Ndibewu, M. M. Kalumba, N. A. Panichev, H. M. Ngomo, and J. M. Ketcha, "Adsorption of mercury(II) onto activated carbons derived from theobroma cacao pod

husk S," *African Journal of Chemistry*, vol. 68, pp. 226–235, 2015.

[45] H. I. Maarof, B. H. Hameed, and A. L. Ahmad, "Adsorption equlibrium of phenols from aqueous solution using modified clay," *Journal Jurutera Kimia Malaysia*, vol. 3, pp. 85–96, 2003.

[46] S. Asgari, M. A. Sahari, and M. Barzegar, "Ultrasound-assisted bleaching of olive oil: kinetics, isotherms and thermodynamics," *Journal of Food Engineering*, vol. 224, pp. 37–44, 2018.

[47] Z. Wu and C. Li, "Kinetics and thermodynamics of -carotene and chlorophyll adsorption onto acid-activated bentonite from Xinjiang in xylene solution," *Journal of Hazardous Materials*, vol. 171, no. 1-3, pp. 582–587, 2009.

[48] R. S. Pohndorf, T. R. S. Cadaval, and L. A. A. Pinto, "Kinetics and thermodynamics adsorption of carotenoids and chlorophylls in rice bran oil bleaching," *Journal of Food Engineering*, vol. 185, pp. 9–16, 2016.

[49] E. S. Almeida, A. C. B. Carvalho, I. OdS. Soares et al., "Elucidating how two different types of bleaching earths widely used in vegetable oils industry remove carotenes from palm oil: equilibrium, kinetics and thermodynamic parameters," *Food Research International*, vol. 121, pp. 785–797, 2019.

[50] M. A. Conde, C. L. S. Liwaire, A. N. Tchakounte, A. S. Ntinkam, D. L. E. Nzugue, and C. M. Kede, "Removal of methyl orange (MO) by chitosan modified by zero valent iron," *International Journal of Engineering Research and Technology*, vol. 9, no. 7, pp. 1542–1549, 2020.

[51] B. H. Hameed, D. K. Mahmoud, and A. L. Ahmad, "Equilibrium modeling and kinetic studies on the adsorption of basic dye by a low-cost adsorbent: coconut (*Cocos nucifera*) bunch waste," *Journal of Hazardous Materials*, vol. 158, no. 1, pp. 65–72, 2008.

[52] H. Lalhruaitluanga, K. Jayaram, M. N. V. Prasad, and K. Kumar, "Lead(II) adsorption from aqueous solutions by raw and activated charcoals of melocanna baccifera roxburgh (bamboo)—a comparative study," *Journal of Hazardous Materials*, vol. 175, no. 1–3, pp. 311–318, 2010.

[53] S. Piri, Z. A. Zanjani, F. Piri, A. Zamani, M. Yaftian, and M. Davari, "Potential of polyaniline modified clay nanocomposite as a selective decontamination adsorbent for Pb(II) ions from contaminated waters; kinetics and thermodynamic study," *Journal of Environmental Health Science and Engineering*, vol. 14, no. 1, p. 20, 2016.

[54] P. P. Ndibewu, C. M. Kede, P. G. Tchieta, H. Z. Poumve, and A. N. Tchakounte, "Simultaneous adsorption of mercury (II) and zinc (II) ions from aqueous solution onto activated carbons derived from a lowland bioresource waste," *Journal of Applied Surfaces and Interfaces*, vol. 5, 2019.

[55] B. Kakavandi, R. R. Kalantary, M. Farzadkia et al., "Enhanced chromium(VI) removal using activated carbon modified by zero valent iron and silver bimetallic nanoparticles," *Journal of Environmental Health Science and Engineering*, vol. 12, no. 1, p. 115, 2014.

[56] B. V. Devi, A. Jahagirdar, and M. Z. Ahmed, "Adsorption of chromium on activated carbon prepared from coconut shell," *Adsorption*, vol. 2, 2012.

[57] M. Jamshidi, M. Ghaedi, K. Dashtian, S. Hajati, and A. A. Bazrafshan, "Sonochemical assisted hydrothermal synthesis of ZnO: Cr nanoparticles loaded activated carbon for simultaneous ultrasound-assisted adsorption of ternary toxic organic dye: derivative spectrophotometric, optimization, kinetic and isotherm study," *Ultrasonics Sonochemistry*, vol. 32, pp. 119–131, 2016.

[58] S. P. Shella, A. E. Angkawijaya, M. Yuliana et al., "Saponin-intercalated organoclays for adsorptive removal of β-carotene, reusability, and phytotoxicity assessment," *Journal of the Taiwan Institute of Chemical Engineers*, pp. 1–11, 2020.

[59] R. O. Ajemba and O. D. Onukwuli, "Adsorptive removal of colour pigment from palm oil using acid activated nteje clay kinetics, equilibrium and thermodynamics," *Physicochemical Problems of Mineral Processing*, vol. 49, no. 1, pp. 369–381, 2013.